Nonlinear Forced Vibration Analysis of Dielectric-Elastomer Based Micro-Beam with Considering Yeoh Hyper-Elastic Model

Abstract

The present study investigates nonlinear forced vibration of dielectric elastomer–based micro-beam. The nonlinear terms in beam equation are geometric and material one. Geometric nonlinearity is considered by von-Karman strain displacement relationship and the material nonlinearity is modeled with Yeoh hyper-elastic model. Galerkin and Multiple scale methods solve the governing equation. This solution that includes primary resonance, leads to frequency response, so that we depict influence of detuning parameter on amplitude in variation of different parameters.

Keywords

Hyper-elastic, Yeoh, Micro-beam, Euler-Bernoulli, Primary resonance

Ardeshir Karami Mohammadi [a]
Saeed Danaee Barforooshi [b]

[a] Department of Mechanical Engineering, Shahrood University of Technology, Shahrood, Iran, P.O.B 3619995161
akaramim@yahoo.com
[b] Department of Mechanical Engineering, Shahrood University of Technology, Shahrood, Iran, P.O.B 3619995161
saeeddanaee@gmail.com

1 INTRODUCTION

Electro-active polymers (EAP) are polymers that undergo size or shape changes when encounter electrical stimulation. Currently these polymers have attracted attention of researchers around the world. Dielectric elastomers (DEs) belong to the group of electro-active polymers. They are lightweight, have a high elastic energy density, and product large strains. Also potential of chemical and biological compatibility, simplicity of structure and robustness due to the use of stable and commercial availability are the other properties that make dielectric elastomers good candidate for applications such as artificial muscles, sensors, generators, loud speakers, micro air vehicles, energy harvesting, haptic surfaces, actuators and resonators (Zhigang, 2010; Mockenstrum and Goulbourne, 2006; Feng and Zhang, 2014; Carpi et al.,2011; Stoyanov et al., 2009; Chakravarty, 2014; Cohen, 2004).
DEs are hyper-elastic materials and we should consider material nonlinearity in their modeling, The material nonlinearity due to nonlinear stress- strain relationship can be modeled using various hy-

perelastic constitutive models. These models can be classified into two main formulations based on the strain energy functions: (1) phenomenological models such as Mooney, Mooney-Rivlin, Bidermann, Yeoh, and Ogden model. (2) Physically-based models such as Neo-Hookean, Isihara model, and Slip-Link model (Markmann and Verron, 2006). These models were used by some researchers in different cases. Here the most important works have been reviewed.

Yeoh (1990) represented a strain energy function which was cubic in I_1 . This function proposed for the characterization of the elastic properties of carbon-black-filled rubber vulcanizates and included variable shear deformation. The use of proposed strain-energy function has been shown to permit the prediction of stress-strain behavior in different deformation modes, from data obtained in one simple deformation mode.

Ogden and Roxburgh (1993) studied plane vibrations superimposed on the homogeneous deformation of a rectangular block of incompressible isotropic elastic material. They obtained frequency equations in respect of a general form of strain-energy function. Their interest was the case of zero frequency, because of occurrence of bifurcation equations that each of them determines a set of values of deformation and stress. Also they illustrated dependency of frequency on the deformation, stress and aspect ratio.

Verron et al. (1999) studied dynamic inflation of hyper-elastic spherical membranes with Mooney–Rivlin material. In addition, they examined the conditions for oscillatory inflation around the static fixed point and found that the frequency of oscillation reaches a maximum at some pressure level, which tends to increase for materials with Neo-Hookean material.

Ogden et al. (2004) concerned determining material parameters in incompressible isotropic elastic strain-energy functions based on a non-linear least squares optimization method by fitting data from the classical experiments of Treloar and Jones on natural rubber. They considered three separate forms of strain-energy function: principle stretches, principle invariants of Cauchy-Green deformation tensor and a certain set of orthogonal invariants of the logarithmic strain tensor. They showed that at least in the case of elastomeric materials, it is advisable to examine their behavior first via mathematical models rather than by simulation models.

Mason and Maluleke (2007) showed that when the strain energy function is specified as Mooney-Rivlin strain energy function, three second order equations are derived for radial oscillations in a thin-walled tube. In addition, they concluded that existence of one Lie point symmetry in presence of time dependent net applied force is only for special forms of the generalized Mooney-Rivlin strain energy function and for special net applied surface pressure.

Lopez-Pamies (2010) proposed a new hyperelastic model, which was applicable over the whole range of deformations. His model like Yeoh model was based on first invariant strain but with a real number as a power. The proposed stored-energy function in his research constituted a practical platform from which to account for more levels of complexity to model rubber solids.

Zhu et al. (2010) analyzed nonlinear dynamics of a membrane of a dielectric elastomer. Some of their concluding remarks are as follow: when the fundamental natural frequency vanishes, state of equilibrium would be unstable; the natural frequencies of dielectric elastomers were tunable by varying the pre-stretch, pressure, or voltage, when driven by a sinusoidal voltage; the membrane resonated at multiple values of the frequency of excitation when driven by a sinusoidal voltage.

Steinmann et al. (2012) reviewed fourteen selected of hyperelastic models and derived analytical stress-stretch relations for certain homogeneous deformation modes. Furthermore they evaluated validity of the models with regard to the classical experimental data on vulcanized rubber published by Treloar. Also they derived ingredient necessary for their fitting procedures for all fourteen models.

Patil and Dasgupta (2013) studied finite axisymmetric inflation of an initially stretched flat circular hyperelastic membrane. Membrane's material was isotropic Mooney-Rivlin solid. The aim of their work had been to study the inflation of hyperelastic membrane and distinguish between the effects of pre-stretch and internal pressure on the inflation mechanics. They observed that softening or stiffening of a membrane and the limit point pressure depends on material model and pre-stretch. Their solution could be used to study inflation assisted thermoforming and angioplasty.

Breslavsky et al. (2014) investigated static deflection, free and forced vibrations of thin rubber plates. This rectangular plate was under uniformly distributed pressure. Physical and geometrical nonlinearity were introduced by neo-hookean model and von Karman strains, respectively. Comparison of their result with exact solution, validated corresponding results. They showed that sensitivity of the deflection to the physically induced nonlinearities at moderate strain is significant.

Feng et al. (2014) studied the dynamic properties of a dielectric elastomer (DE)-based micro-beam resonator with ambient pressure that was affected by using the squeeze-film theory. They approximated analytical solutions for the quality factor and the resonant frequencies. Their results exhibited that the ambient pressure has significant effects on the Q-factor and the resonant frequency shift ratio.

Bhattacharyya et al. (2015) did their research in particular about instability of the steady state balloons. The material was neo-Hookean rubber. They used shooting method for obtaining steady state results. Theoretical results showed that the single loop balloons have higher tension and they are always stable. Also they depicted the effect of material nonlinearity in steady state curves.

Pineda et al. [20] used from hyper-elastic polymer for the improvement of soft sensors with large deformation. They combined hyper-elastic materials and conductive fluid to allow the expansion of sensors with enormous deformation. They demonstrated that these sensors are reliable even after several cycles.

Rodriguez-Martinez et al. (2015) investigated dependency of stability of hyper-elastic spherical membrane on constitutive models. They considered six strain-energy functions: three of the Mooney-Rivlin type and three of the Ogden type. Significant influence of constitutive models on mechanical stability of rubber-like balloons subjected to dynamic loadings was shown. They observed that the steady response of the membrane is extremely conditioned by the strain-energy function selected. In addition they discussed about reduction of uncertainty surrounding the dynamic modeling of rubber-like materials.

Danaee Barforooshi and Karami Mohammadi (2016) considered a micro-bridge resonator with geometric and material nonlinearity. Geometric nonlinearities were introduced by von-Karman strains and for material nonlinearity the Yeoh and neo-Hookean models were used. They showed that neo-Hookean model is not suitable for this case, because of insufficient terms in its strain-energy function. Perturbation technique was used for solution of the nonlinear governing equation

and good agreement was achieved between analytical and numerical results. The results showed the significant influence of mode number on the normalized frequencies.

Madireddy et al. (2015) studied the use of Bayesian approach to estimate the hyper-elastic material parameters for sift tissue. They considered Mooney-Rivlin, exponential and Ogden model to represent hyper-elastic nature of soft tissue. They showed that the quality of the fit alone is inadequate to find out the sufficiency of the model. Also, they observed the importance of taking into account the noise and uncertainty in the data in constructing material models.

In this work, dielectric elastomer-based micro-beam is considered as a resonator. The Yeoh hyper-elastic model is used to describe the material nonlinearity and the von-Karman strains are used to consider large deformations. This micro-beam is simply supported at the ends and Multiple-scale method is used for solving governing equation.

2 EQUATION OF MOTION

As shown in Fig.1, simply supported Dielectric elastomer-based micro-beam has length L , height d , width b .
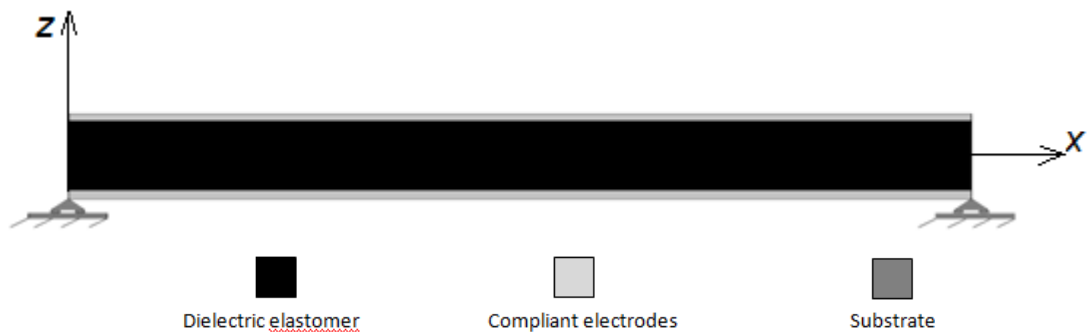

Figure 1: Schematic of micro-beam.

The equation of motion is derived under the following assumptions: (1) the cross-section of micro-beam is constant over the entire length; (2) the extended Euler-Bernoulli beam theory can be applied; (3) geometric and material nonlinearities are considered due to large deformation and hyperelastic behavior, respectively.

Displacement field for a Euler-Bernoulli beam is:

$$u = -z \frac{\partial w(x,t)}{\partial x}, \quad v = 0, \quad w = w(x,t) \tag{1}$$

where z is the vertical distance of every point of the beam to neutral axis, u is the axial displacement of the point, and w denotes the lateral deflection of the beam.

According to large deformation, Green-Lagrange strain deformation is used:

$$\varepsilon_{ij} = \frac{1}{2} \left(\frac{\partial u_i}{\partial x_j} + \frac{\partial u_j}{\partial x_i} + \frac{\partial u_k}{\partial x_j} \frac{\partial u_k}{\partial x_i} \right) \tag{2}$$

Then, the von-Karman strain components are:

$$\varepsilon_{11} \approx -z\frac{\partial^2 w}{\partial x^2} + \frac{1}{2}\left(\frac{\partial w}{\partial x}\right)^2$$

$$\varepsilon_{13} = \varepsilon_{31} = \varepsilon_{33} \approx 0 \tag{3}$$

$$\varepsilon_{12} = \varepsilon_{21} = \varepsilon_{22} = \varepsilon_{23} = \varepsilon_{32} = 0$$

Yeoh developed a hyper-elastic material model that only depends on the first strain invariants. This model is based on a series expansion and its series is truncated after the first three terms. Therefore, its strain energy density function is:

$$W = \sum_{i=1}^{3} c_i\,(\mathrm{I}_1 - 3)^i \tag{4}$$

Where c_i are material constants and I_1 is the first strain invariant that is related to principle stretches and right Cauchy- Green strain tensor as follows:

$$I_1 = \lambda_1^2 + \lambda_2^2 + \lambda_3^2 = tr(\mathrm{C}) \tag{5}$$

It should be mentioned that $\lambda_i\,(i=1,2,3)$ are square root of the right Cauchy- Green strain tensor (C) and C is related to strain tensor, E, that its components are introduced in equation (3).

$$C = 2E + I \tag{6}$$

Using potential energy as

$$\Pi = \int_V W dV \tag{7}$$

Substituting from equations (4), (5) and (6) into (7), leads to the potential energy as a function of *w*. Also, kinetic energy can be written as follows:

$$T = \frac{1}{2}\int_0^l \rho A(\frac{\partial w}{\partial t})^2\, dx \tag{8}$$

Substituting potential and kinetic energies and considering a distributed frequency force into extended Hamilton principle, leads to following governing equation:

$$\rho A\frac{\partial^2 w}{\partial t^2} + 8c_2 I\frac{\partial^4 w}{\partial x^4} + 24c_3 I\frac{\partial^4 w}{\partial x^4}\left(\frac{\partial w}{\partial x}\right)^2 + 96c_3 I\frac{\partial^3 w}{\partial x^3}\frac{\partial^2 w}{\partial x^2}\frac{\partial w}{\partial x}$$

$$-2c_1 A\frac{\partial^2 w}{\partial x^2} - 12c_2 A\frac{\partial^2 w}{\partial x^2}\left(\frac{\partial w}{\partial x}\right)^2 - 30c_3 A\frac{\partial^2 w}{\partial x^2}\left(\frac{\partial w}{\partial x}\right)^4 \tag{9}$$

$$+24c_3 I\left(\frac{\partial^2 w}{\partial x^2}\right)^3 = f_0\cos(\Omega t)$$

with boundary conditions $w(0) = 0,\ w(L) = 0,\ \dfrac{\partial w}{\partial x}(0) = 0,\ \dfrac{\partial w}{\partial x}(L) = 0$.

Equation of motion and boundary conditions can be normalized with proper non-dimensional parameters:

$$x^* = \frac{x}{l}, \quad w^* = \frac{w}{d}, \quad t^* = t\omega_{\dim}, \quad \Omega^* = \frac{\Omega}{\omega_{\dim}} \tag{10}$$

$\omega_{\dim}$ is the linear dimensional natural frequency of micro-beam that is achieved by linearization of equation (9).

Therefore, we have:

$$
\begin{aligned}
&\frac{\partial^2 w^*}{\partial t^{*2}} + \beta_1 \frac{\partial^4 w^*}{\partial x^{*4}} + \beta_2 \frac{\partial^4 w^*}{\partial x^{*4}}\left(\frac{\partial w^*}{\partial x^*}\right)^2 + 4\beta_2 \frac{\partial^3 w^*}{\partial x^{*3}}\frac{\partial^2 w^*}{\partial x^{*2}}\frac{\partial w^*}{\partial x^*} \\
&-\beta_3 \frac{\partial^2 w^*}{\partial x^{*2}} - \beta_4 \frac{\partial^2 w^*}{\partial x^{*2}}\left(\frac{\partial w^*}{\partial x^*}\right)^2 - \beta_5 \frac{\partial^2 w^*}{\partial x^{*2}}\left(\frac{\partial w^*}{\partial x^*}\right)^4 \\
&+\beta_2 \left(\frac{\partial^2 w^*}{\partial x^{*2}}\right)^3 = F_0 \cos(\Omega^* t^*)
\end{aligned}
\tag{11}
$$

where

$$\beta_1 = \frac{8c_2 I}{\rho A L^4 \omega_{\dim}^2},\ \beta_2 = \frac{24c_3 d^2 I}{\rho A L^6 \omega_{\dim}^2},\ \beta_3 = \frac{2c_1}{\rho L^2 \omega_{\dim}^2},\ \beta_4 = \frac{12c_2 d^2}{\rho L^4 \omega_{\dim}^2},\ \beta_5 = \frac{30c_3 d^4}{\rho L^6 \omega_{\dim}^2},\ F_0 = \frac{f_0}{\rho A d \omega_{\dim}^2} \tag{12}$$

and normalized boundary conditions $w(0) = 0,\ w(1) = 0,\ \dfrac{\partial w}{\partial x}(0) = 0,\ \dfrac{\partial w}{\partial x}(1) = 0$.

Reduced Order Model

For solving nonlinear PDE equation, first the Galerkin method is used to reduce the equation to ODE one. So the function will be introduced as multiplication of two separated spatial and time functions as:

$$w^*(x^*, t^*) = X(x^*)q(t^*), \quad X(x^*) = \sqrt{2}\sin(m\pi x^*) \tag{13}$$

Now with multiplying mode shape function in each side of equation (11) and integrating from zero to one, the achieved ODE equation will be:

$$\ddot{q}(t^*) + \alpha_1 q(t^*) + \alpha_2 q^3(t^*) + \alpha_3 q^5(t^*) = F_0 \cos(\Omega^* t^*) \tag{14}$$

where

$$\alpha_1 = \beta_1 m^4 \pi^4 + \beta_3 m^2 \pi^2 \tag{15}$$

$$\alpha_2 = \beta_2 m^6 \pi^6 + \frac{\beta_4}{2} m^4 \pi^4$$

$$\alpha_3 = \frac{\beta_5}{2} m^6 \pi^6$$

Multiple Scale Method

One of the strong perturbation methods for solving nonlinear equations is the well-known multiple scale method (Nayfeh, 1979). To use this approach, small perturbation parameter, $q = \varepsilon u$, is introduced, moreover, the scaled time can be introduced as:

$$T_n = \varepsilon^n t^* \tag{16}$$

The proposed solution is:

$$u = u_0(\mathrm{T}_0, \mathrm{T}_1, \mathrm{T}_2) + \varepsilon u_1(\mathrm{T}_0, \mathrm{T}_1, \mathrm{T}_2) + \varepsilon^2 u_2(\mathrm{T}_0, \mathrm{T}_1, \mathrm{T}_2) \tag{17}$$

Substituting equations (16) and (17) into equation (14) and arranging based on different orders of ε^i by Maple software; the following perturbation equations are obtained:

$$\varepsilon^1 : \frac{\partial^2 u_0}{\partial T_0^{\,2}} + \alpha_1 u_0 = 0 \tag{18}$$

$$\varepsilon^2 : \frac{\partial^2 u_1}{\partial T_0^{\,2}} + \alpha_1 u_1 + 2 \frac{\partial^2 u_0}{\partial T_0 \partial T_1} = 0 \tag{19}$$

$$\varepsilon^3 : \frac{\partial^2 u_2}{\partial T_0^{\,2}} + \alpha_1 u_2 + 2 \frac{\partial^2 u_1}{\partial T_0 \partial T_1} + \alpha_2 u_0^3 + \frac{\partial^2 u_0}{\partial T_1^2} + 2 \frac{\partial^2 u_0}{\partial T_0 \partial T_2} = F_0 \cos(\Omega^* \mathrm{T}_0) \tag{20}$$

For eliminating small divisor terms, the force term should be placed in the largest order of ε. It should be noted that α_1 is equal to square of non-dimensional linear frequency ($\alpha_1 = \omega_0^{\,2}$)

The solution of equation (18) can be supposed as:

$$u_0 = A(\mathrm{T}_1, \mathrm{T}_2) \mathrm{e}^{i\omega_0 T_0} + cc \tag{21}$$

where cc stands for "complex conjugate" of the first term.

Substituting equation (21) into equation (19) and eliminating secular terms, leads to:

$$D_1 A = 0 \rightarrow A = A(\mathrm{T}_2) \tag{22}$$

$$u_1 = 0 \tag{23}$$

Now substitution of equations (21) and (23) into equation (20) yields:

$$D_0^{\,2} u_2 + \omega_0^{\,2} u_2 + 2\left(i\omega_0 A' \mathrm{e}^{i\omega_0 T_0} + i\omega_0 \overline{A}' \mathrm{e}^{-i\omega_0 T_0} \right) + \alpha_2 \left(A \mathrm{e}^{i\omega_0 T_0} + \overline{A} \mathrm{e}^{-i\omega_0 T_0} \right)^3 = \frac{F_0}{2} \left(\mathrm{e}^{i\Omega^* T_0} + \mathrm{e}^{-i\Omega^* T_0} \right) \tag{24}$$

To consider primary resonance, we introduce a detuning parameter σ defined by:

$$\Omega^* = \omega_0 + \varepsilon^2 \sigma \tag{25}$$

And when $\sigma \to 0$, excitation frequency tends to linear natural frequency. Then

$$\Omega^* T_0 = (\omega_0 + \varepsilon^2 \sigma) T_0 = \omega_0 T_0 + \varepsilon^2 \sigma T_0 = \omega_0 T_0 + \sigma T_2 \tag{26}$$

Substituting equation (26) into equation (24) and eliminating secular terms, results in:

$$3\alpha_2 A^2 \overline{A} + 2i\omega_0 A' - \frac{F_0}{2} e^{i\sigma T_2} = 0 \tag{27}$$

Consider the polar form for A:

$$A = \frac{1}{2} a \, e^{i\beta} \tag{28}$$

And substituting equation (28) into (27), multiplying each side by $e^{-i\beta}$ and finally separating real and imaginary parts, yields:

$$\frac{3}{8}\alpha_2 a^3 - \omega_0 a \beta' - \frac{F_0}{2}\cos(\sigma\, T_2 - \beta) = 0 \tag{29-1}$$

$$\omega_0 a' - \frac{F_0}{2}\sin(\sigma\, T_2 - \beta) = 0 \tag{29-2}$$

We transform equations (29) into an autonomous system by introducing the transformation:

$$\sigma\, T_2 - \beta = \gamma \tag{30}$$

And taking derivative yields:

$$\sigma - \beta' = \gamma' \tag{31}$$

Substituting equations (30) and (31) into equations (29) and after some algebra, the frequency response is obtained as:

$$\left(\frac{3}{8}\alpha_2 a^3 - \omega_0 \sigma a\right)^2 = \frac{F_0^2}{4} \tag{32}$$

It should be noted that in steady state solution: $a' = \gamma' = 0$

Analytical solution of governing nonlinear ordinary differential equation with substation of equations (21) and (23) into (17), will be:

$$q(t^*) = \varepsilon a \cos(\omega_0 t^* + \beta) + O(\varepsilon^3) \tag{33}$$

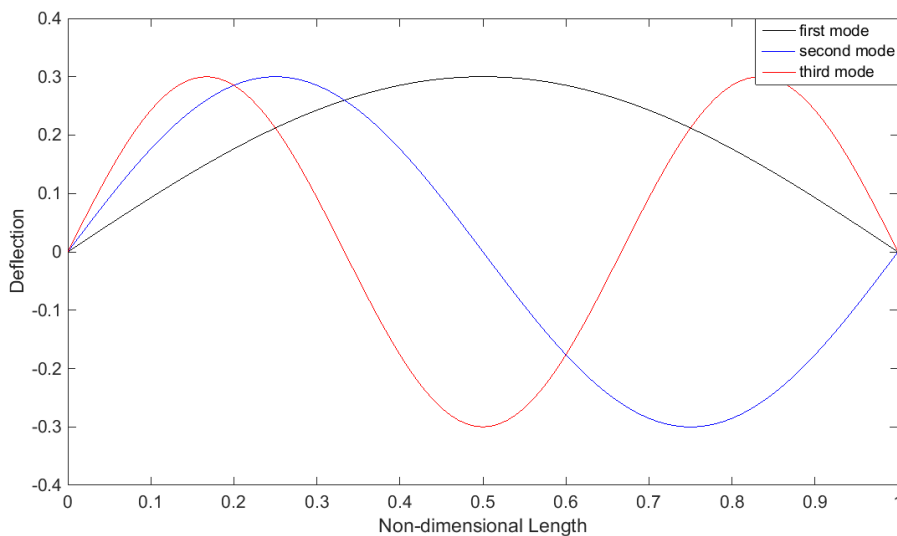## Mode Shapes and Frequency Response Curves

In this section, a case study has been prepared using geometrical and material properties introduced in table (1). Material constants are based on uni-axial tension test (Martins et al, 2006).

Geometric properties	Material properties
$l = 30\,\mu m$	$c_1 = 0.24162\,MPa$
$b = 10\,\mu m$	$c_2 = 0.19977\,MPa$
$d = 0.65\,\mu m$	$c_3 = -0.00541\,MPa$

Table 1: Micro-beam geometrical and material properties.

Respect to relation (25) the first three non-dimensional natural frequencies, Ω^*, at $\sigma = 0$ attain 0.0717, 0.1448 and 0.2207, respectively.

Figure (1) shows midpoint displacement versus non-dimensional length for different modes. As it is seen, the ends of the micro-beam are in agreement with boundary conditions. It should be mentioned that non-dimensional maximum amplitude is 0.3 ($w^*_{max} = 0.3$) for large deflection of the midpoint and is introduced by initial conditions.


Figure 2: Mode shape of the micro-beam for the first three modes.

The frequency response curves in non-dimensional amplitude-detuning parameter plane are presented around its first natural frequency. These curves depicted by spanning the excitation frequency (Ω) around the first linear natural frequency. With the aid of these curves, the hardening or softening types of behavior in this micro-beam can be determined.

Figures (3), (4) and (5) show variation of midpoint amplitude versus detuning parameter for the first, second and third mode of transverse motion, respectively. These figures are depicted based on frequency response introduced in equation (32). As it is seen, as the detuning parameter ap-

proaches to zero, the amplitude of motion is increased because of nearness of excitation frequency to the linear natural frequency. This rising continues until the first limit point bifurcation at the top and reaches to maximum amplitude. At this point the system response will be unstable. Stable parts are shown with solid line and the unstable one is shown with dash line. From these figures, it is clear that the system behavior is of hardening type. The maximum amplitude in the figures (3), (4) and (5), at the resonance frequency tends to reach 2205, 777 and 421, respectively.

In addition, the higher mode number is related to hardener behavior of micro-beam.
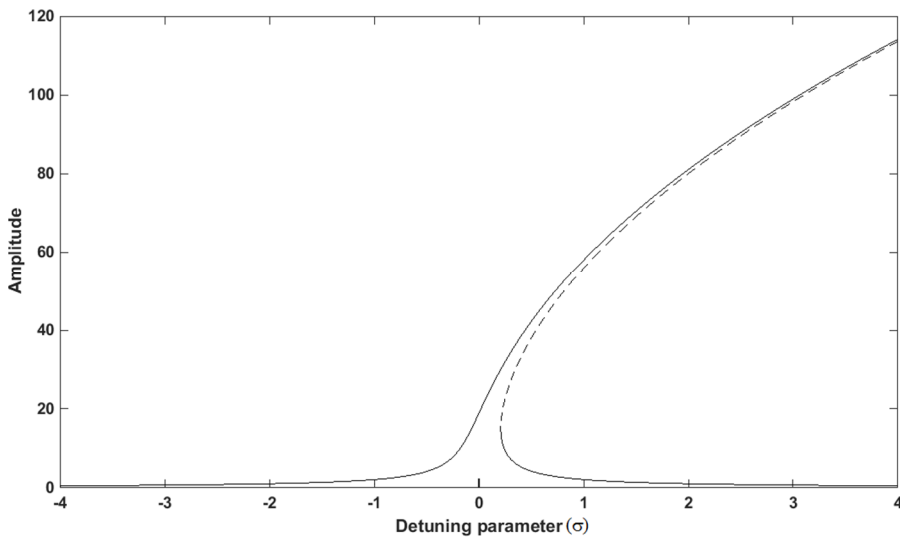
Figure 3: Bifurcation diagram for the first mode.
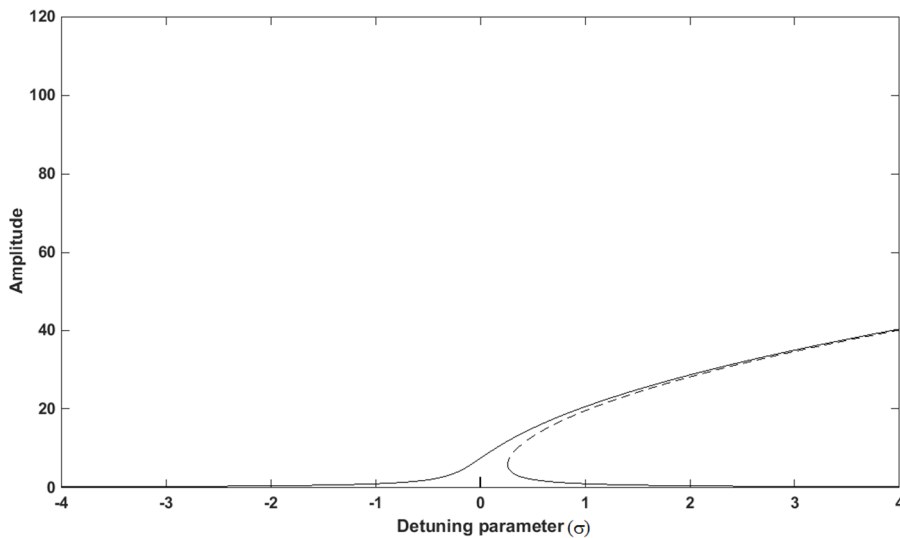
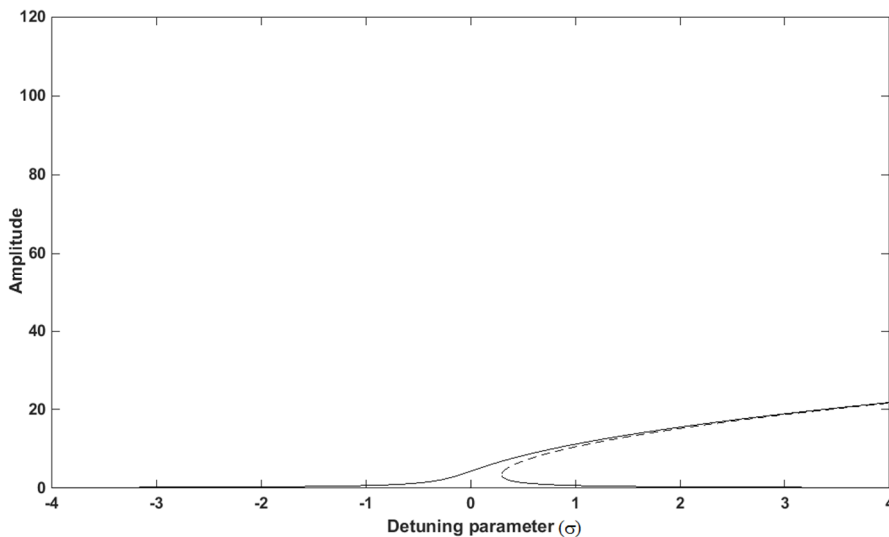**Figure 4**: Bifurcation diagram for the second mode.

Figure 5: Bifurcation diagram for the third mode.

Figures (6)-(8) show bifurcation diagrams for different lengths in terms of constant thickness. It is obvious that maximum amplitude is larger and resonance is more intensive in beams with higher aspect ratio ($\frac{L}{d}$).

For all modes, the behavior of micro-beam gets hardener as the length gets shorter (smaller aspect ratio).

The maximum amplitude at the resonance for the $L = 50\,\mu m$, $40\,\mu m$ and $30\,\mu m$ in figures (6), (7) and (8) tends to reach [4747, 3396 and 2205],[1676, 1199,777] and [911, 651, 421], respectively.
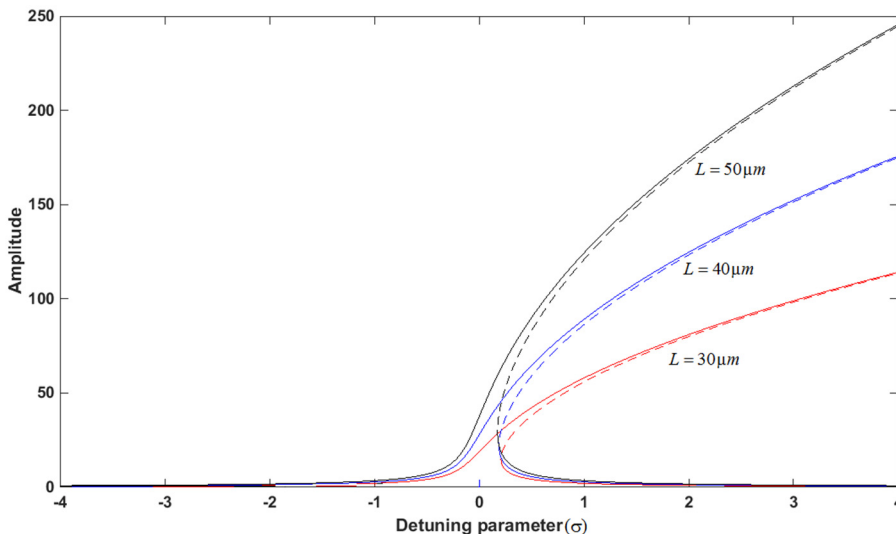

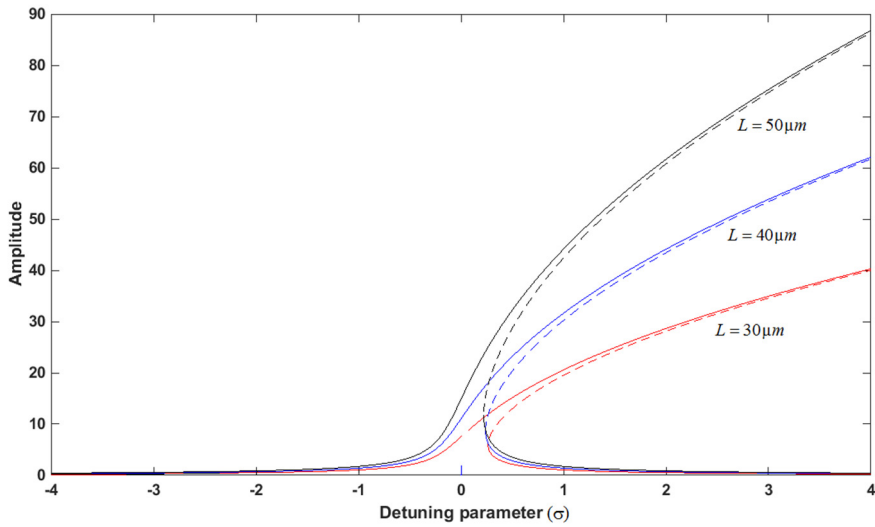**Figure 6**: Bifurcation diagram for different lengths at first mode.

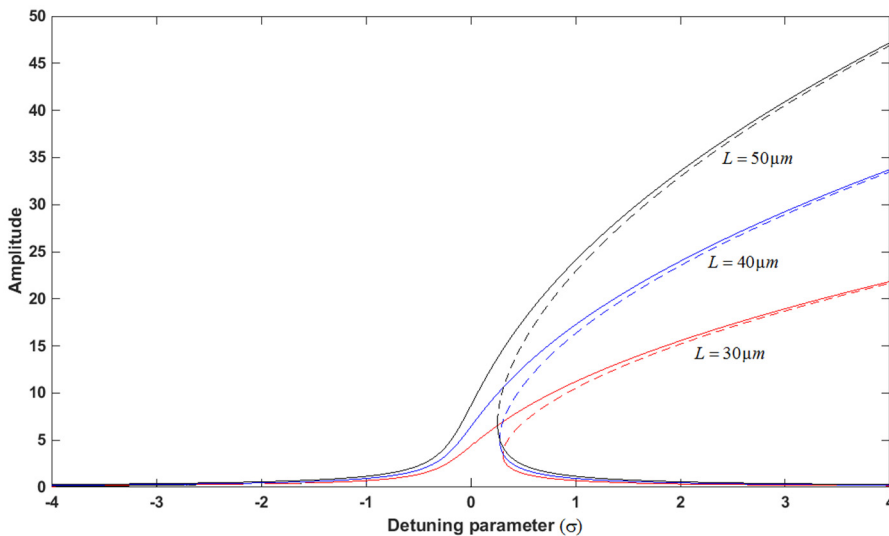**Figure 7**: Bifurcation diagram for different lengths at second mode.

Figure 8: Bifurcation diagram for different lengths at third mode.

In figures (9) and (10), influence of the non-dimensional amplitude of external harmonic force on the bifurcation diagram is depicted. Two different quantities are chosen here for the force amplitude in each mode. One can observe that for larger force amplitudes, the first stable part is began to rise at smaller detuning parameter and the second stable part is terminated in larger detuning parameter. It means that maximum amplitude occurs at higher excitation frequencies. In addition, the forcing amplitude leads to larger hardening behavior at higher modes.

The maximum amplitude at the resonance for the first and second mode in figure (9) tends to reach 2204 and 777, respectively.
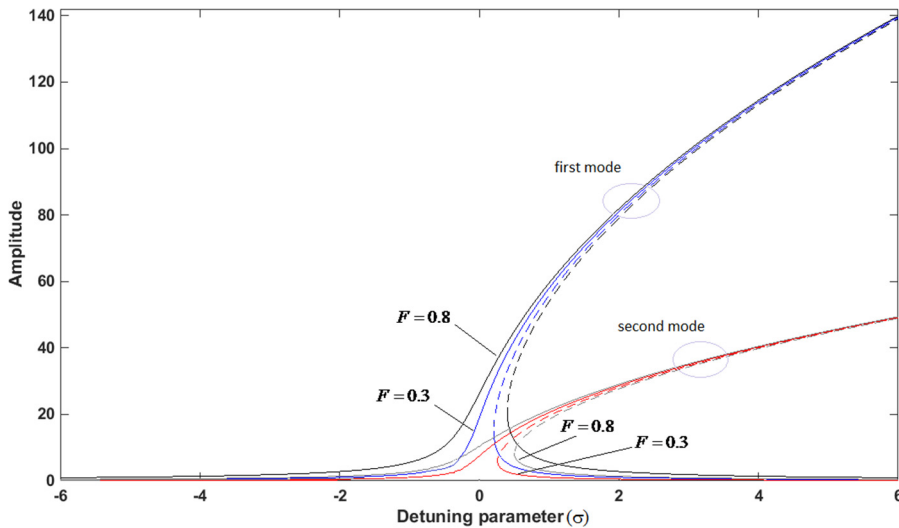
Figure 9: Influence of force amplitude on micro-beam behavior.

3   CONCLUSIONS

A micro-beam with material in the class of Electro-active polymers (Dielectric elastomer) was the case in this study. The nonlinearity that considered here was geometric and material one. Geometric nonlinearity modeled via von-Karman strain-displacement relationship and Material nonlinearity was based on Yeoh hyper-elastic model. The nonlinear governing equation solved by Galerkin and Multiple-scale methods. Influence of different parameters on amplitude-detuning parameter diagram at primary resonance was studied. Some conclusions and remarks that have been evolved in this article:

- Dielectric elastomer-based micro-beam with Yeoh model has hardening behavior.
- Higher mode number has a direct effect on hardening behavior of DE micro-beam.
- Higher of mode number has an inverse effect on amplitude of motion.
- Higher aspect ratio leads to higher amplitude of motion at all modes.
- Shorter beams have more harden behavior.
- Magnitude of force amplitude has direct effect on the rise beginning of bifurcation diagram.
- The forcing amplitude leads to larger hardening behavior at higher modes.

References:

Bhattacharyya, R. Sarangi, S. Samantaray, A.K. (2015), Effect of stress-softening on the ballooning motion of hyperelastic strings. International Journal of Engineering Scienece. 96: 19-33.

Breslavsky, I.D. Amabili, M Legrand, M., (2014). Physically and geometrically non-linear vibrations of thin rectangular plates. Internationa Journal of Non-Linear Mechanics, 58: 30-40.

Carpi, F., De Rossi, D., Kornbluh, R., Pelrine, R.E., Sommer-Larsen,P. (2011). Dielectric elastomers as electromechanical transducers: Fundamentals, materials, devices, models and applications of an emerging electroactive polymer technolo-gy. Elsevier.

Chakravarty, U. K., (2014). On the resonance frequencies of a membrane of a dielectric elastomer. Mechanics Research Communications 55.1: 72– 76.

Cohen, Y.B., (2004). Electro-active polymer (EAP) actuators as artificial muscles: reality, potential and challenges, SPIE Press.

Danaee. Barforooshi, S., Karami Mohammadi, A. (2016). study neo-Hookean and Yeoh hyper-elastic models in dielectric elastomer-based micro-beam resonators. 13: 1823-1837.

Feng, C. Yu, L. and Zhang, W., (2014). Dynamic analysis of a dielectric elastomer-based microbeam resonator with large vibration amplitude, Int. Journal Nonlinear Mechanics. 65: 63-68.

Lopez-Pamies, O., (2010). A new I_1 - based hyperelastic model for rubber elastic materials, Comptes Rendus Mechanique, 338:2-11.

Markmann, G.,Verron, E., (2006). Comparision of hyperelastic models for rubber-like materials, Rubber Chemistry and Technology. 79.5: 835-858.

Martins, P. A. L. S. R, Natal Jorge, M, and Ferreira, A. J. M. A., (2006). Comparative Study of Several Material Models for Prediction of Hyperelastic Properties: Application to Silicone-Rubber and Soft Tissues, , Strain Journal, 42: 135-147.

Mason, D.P., Maluleke, G.H. (2007). Non-linear radial oscillations of a transversely isotropic hyperelastic incompressible tube. Journal of Applied Mathematics and applications. 333.1: 365–380.

Mockenstrum, E.M. and Goulbourne, N., (2006), Dynamic response of dielectric elastomers, Int. Journal Nonlinear Mechanics. 41: 388-395.

Nayfeh, A.H. (1979). Nonlinear oscillations, John Wiley and sons, New York.

Ogden, R.W. and Roxburgh, D.G., (1993). The effect of pre-stress on the vibration and stability of elastic plates. Int. Journal of Engineering Science., 31 pp. 1611- 1639.

Ogden, R.W., Saccomandi, G., Sgura, I. (2004). Fitting hyperelastic models to experimental data. Computational Mechan-ics, 34.6: 484-502.

Patil. A. .DasGupta, A,. (2013). Finite inflation of an initially stretched hyperelastic circular membrane, European Journal of MechanicsA/solids . 41: 28-36

Pineda, F, Bottausci, F, Icard, B, Malaquin, L, Fouillet, Y. (2015). Using electrofluidic devices as hyper-elastic strain sensors: Experimental and theoretical analysis. Microelectronic Engineering, 144: 27-31.

Ritto, T.G, Nunes, L.C.S, (2015). Bayesian model selection of hyperelastic models for simple and pure shear at large deformations. Computer and Structures, 156: 101-109.

Rodriguez-Martinez, J.A, Fernandez-Saez, J, Zaera, R. (2015). The role of constitutive relation in the stability of hyper-elastic membranes subjected to dynamic inflation. International Journal of Engineering Science, 93: 31-45.

Steinmann, P. Mokarram. H, gunnar,P. (2012), Hyperelastic models for rubber-like materials: consistent tangent operators and suitability for Treloar's data. Arch Appl Mech, 82: 1183-1217.

Stoyanov, K., H.G., Gerhard, R., (2009). A Co-Axial Dielectric elastomer actuator. Advances in Science and Technology, 61: 81–84.

Verron, E., Khayat, R.E., Derdouri, A., Peseux, B., (1999). Dynamic inflation of hyperelastic spherical membrane. Journal of Rheology. 43.5: 1083-1097.

Yeoh, O.H. (1990), Characterization of elastic properties of carbon-black-filled rubber vulcanizates, Rubber Chemistry and Technology, 63: 792-805.

Zhigang, S., (2010). Theory of dielectric elastomers, Acta. Mech. Solida. Sinica. 23: 549-578.

Zhu, J. Cai, S. and Suo, Z,. (2010). Resonant behavior of a membrane of a dielectric elastomer, Int. J. Solids Struct. 47: 3254–3262.